XVI International Conference on Computational Plasticity. Fundamentals and Applications
COMPLAS 2021
E. Oñate, D. Peric, M. Chiumenti and Eduardo de Souza Neto (Eds)

STAGGERED SCHEME FOR FRACTURE OF BEAM STRUCTURES WITH EMBEDDED STRONG DISCONTINUITIES

VEDAD TOJAGA*, ARTEM KULACHENKO, SÖREN ÖSTLUND AND T. CHRISTIAN GASSER

* Division of Solid Mechanics, Department of Engineering Mechanics
KTH Royal Institute of Technology
SE-100 44 Stockholm, Sweden
e-mail: tojaga@kth.se

Key words: Computational Plasticity, Multi-Fracturing Solids, Embedded Strong Discontinuity, Staggered Solver.

Abstract. We propose a staggered solution scheme for the embedded strong discontinuity finite element method applied to fracture of beam structures, e.g., see our recently accepted paper [1]. We demonstrate the robustness of our implementation for modeling multi-fracturing fibers in random fiber networks loaded in tension. Our implementation enables a user-friendly integration into commercial finite element software. The FORTRAN source code is freely available to benchmark our implementation.

1 INTRODUCTION

The embedded strong discontinuity finite element method [2] has received significant attention in the modeling of fracture in beam structures, e.g., see [3,4]. Advantages include: it does not require a crack tracking algorithm as solids do, it is independent of the size of the characteristic length scale parameter because a fracture process zone is introduced implicitly at the mid-point of the beam finite element, and it is computationally efficient due to the one-dimensional continuum nature of the beam. The method is based on the theory of strong discontinuities where the generalized displacement field $\boldsymbol{u}$ is enhanced by a jump $\boldsymbol{\xi}$ [2]. However, the total potential energy of the enhanced beam formulation is non-convex with respect to the displacement $\boldsymbol{u}$ and the jump $\boldsymbol{\xi}$, leading to the consistent tangent stiffness matrix in Newton's method becoming indefinite, hindering convergence and robustness. In contrast, it is convex with respect to one variable if the other variable is fixed.

For a coupled system, the linearized residual force equations with respect to both unknowns, i.e., the displacement $\boldsymbol{u}$ and the jump $\boldsymbol{\xi}$, using the Newton-Raphson method, take the form

$$\begin{bmatrix} \boldsymbol{K}_{uu} & \boldsymbol{K}_{u\xi} \\ \boldsymbol{K}_{\xi u} & \boldsymbol{K}_{\xi\xi} \end{bmatrix} \begin{bmatrix} \Delta\boldsymbol{u} \\ \Delta\boldsymbol{\xi} \end{bmatrix} = \begin{bmatrix} \boldsymbol{r} \\ \bar{\boldsymbol{r}} = \boldsymbol{0} \end{bmatrix}. \tag{1}$$

Here, $\boldsymbol{K}_{uu}$ is the stiffness matrix of the bulk material, $\boldsymbol{K}_{\xi\xi}$ is the stiffness matrix of the discontinuity, and $\boldsymbol{K}_{u\xi}$ and $\boldsymbol{K}_{\xi u}$ couple the inter-related field. The residual $\bar{\boldsymbol{r}}$ is zero if traction

continuity is enforced between the bulk material and the discontinuity, i.e., $\boldsymbol{K}_{\xi u}\Delta\boldsymbol{u} + \boldsymbol{K}_{\xi\xi}\Delta\boldsymbol{\xi} = \boldsymbol{0}$, e.g., see [4], enabling the static condensation

$$\left(\boldsymbol{K}_{uu} - \boldsymbol{K}_{u\xi}\boldsymbol{K}_{\xi\xi}^{-1}\boldsymbol{K}_{\xi u}\right)\Delta\boldsymbol{u} = \boldsymbol{r} = \boldsymbol{f}_{ext} - \boldsymbol{f}_{int}, \tag{2}$$

$\boldsymbol{f}_{ext}$ and $\boldsymbol{f}_{int}$ being the external and internal force, respectively. The stiffness matrix (2) is non-positive definite and generally non-symmetric, i.e., $\boldsymbol{K}_{\xi u} \neq \boldsymbol{K}_{u\xi}$, e.g., see [4]. The implementation (2) is common in the literature, e.g., see [3–12]. Our own experience using (2) in commercial finite element software was unconvincing as it was not robust in complex multi-fracturing problems.

For a weakly coupled system, the off-diagonal matrices can be removed by neglecting the inter-field coupling, leading to the modified Newton scheme

$$\boldsymbol{K}_{uu}\Delta\boldsymbol{u} = \boldsymbol{r} = \boldsymbol{f}_{ext} - \int \boldsymbol{B}^T\boldsymbol{\sigma}\, dV \quad , \quad \boldsymbol{\sigma} = \boldsymbol{\sigma}(\boldsymbol{u}, \boldsymbol{\xi}), \tag{3}$$

where $\boldsymbol{B}$ is the strain-displacement matrix and $\boldsymbol{\sigma}$ is the stress vector integrated over the volume V of the material, i.e., the internal force. Here, the stiffness matrix (3) is positive definite and symmetric. In (3), we solve the nodal displacement vector $\boldsymbol{u}$ with the jump $\boldsymbol{\xi}_n$ from the previous iteration, followed by the unknown jump $\boldsymbol{\xi}$ with the updated nodal displacement $\boldsymbol{u}$, a procedure repeated until the final solution converges.

We demonstrate the robustness of the weakly coupled embedded strong discontinuity finite element method based on (3) for modeling multi-fracturing fibers in random fiber networks (i.e., the microstructure of paper and other fibrous materials), represented as beam networks, e.g., see [13].

2 THEORY

We consider a 3D Timoshenko beam finite element of the length L and with a symmetric cross-section, where $x \in [0, L]$ is the coordinate along the middle-axis and y, z are mutually orthogonal coordinates to x. The chosen beam finite element has two-node interpolation and one Gauss point for integration. We enhance the generalized displacement field $\boldsymbol{u}_s = \left[u_x\ u_y\ u_z\ \theta_x\ \theta_y\ \theta_z\right]^T$, u for translation and θ for rotation w.r.t. x, y, z, with the displacement/rotation jump $\boldsymbol{\xi} = \left[\xi_{u_x}\ \xi_{u_y}\ \xi_{u_z}\ \xi_{\theta_x}\ \xi_{\theta_y}\ \xi_{\theta_z}\right]^T$ at the mid-point $x = L/2 = x_d$, i.e.,

$$\boldsymbol{u} = \boldsymbol{u}_s + H(x)\boldsymbol{\xi} = N_1\boldsymbol{u}_{s1} + N_2\boldsymbol{u}_{s2} + H(x)\boldsymbol{\xi} = N_1\boldsymbol{u}_1 + N_2\boldsymbol{u}_2 + (H(x) - N_2)\boldsymbol{\xi}, \tag{4}$$

where $N_1 = 1 - x/L$ and $N_2 = x/L$ are linear shape functions and $H(x) = \begin{cases} 0; x \leq x_d \\ 1; x > x_d \end{cases}$ is the Heaviside step function. We impose the boundary conditions $\boldsymbol{u}_1 = \boldsymbol{u}_{s1}$ and $\boldsymbol{u}_2 = \boldsymbol{u}_{s2} + \boldsymbol{\xi}$ to obtain the final result in (4).

From (4), we obtain the enhanced strain field

$$\boldsymbol{\varepsilon} = \boldsymbol{B}\boldsymbol{d} + \boldsymbol{G}\boldsymbol{\xi} + \delta_{x_d}\boldsymbol{\xi}, \tag{5}$$

where $\boldsymbol{G} = \text{diag}[-1/L, -1/L, -1/L, -1/L, -1/L, -1/L]$ is a constant interpolation of the jump $\boldsymbol{\xi}$, $\boldsymbol{B}$ is the strain-displacement matrix

$$\boldsymbol{B} = \begin{bmatrix} B_1 & 0 & 0 & 0 & 0 & 0 & B_2 & 0 & 0 & 0 & 0 & 0 \\ 0 & B_1 & 0 & 0 & 0 & -N_1 & 0 & B_2 & 0 & 0 & 0 & -N_2 \\ 0 & 0 & B_1 & 0 & N_1 & 0 & 0 & 0 & B_2 & 0 & N_2 & 0 \\ 0 & 0 & 0 & B_1 & 0 & 0 & 0 & 0 & 0 & B_2 & 0 & 0 \\ 0 & 0 & 0 & 0 & B_1 & 0 & 0 & 0 & 0 & 0 & B_2 & 0 \\ 0 & 0 & 0 & 0 & 0 & B_1 & 0 & 0 & 0 & 0 & 0 & B_2 \end{bmatrix}, \tag{6}$$

$B_1 = \partial_x N_1 = -1/L$, $B_2 = \partial_x N_2 = 1/L$, $\boldsymbol{d} = [\boldsymbol{u}_1\ \boldsymbol{u}_2]^T$ is the nodal displacement vector, and δ_{x_d} is the Dirac delta function accounting for the deformation at the mid-point x_d.

Given the admissible variations of the displacement $\delta\boldsymbol{d}$ and the jump $\delta\boldsymbol{\xi}$, the internal virtual work of the enhanced beam takes the form

$$\delta w_{int}(\delta\boldsymbol{d}, \delta\boldsymbol{\xi}) = \int_L \delta\boldsymbol{\varepsilon}^T\boldsymbol{\sigma}\, dx = \delta\boldsymbol{d}^T \int_L \boldsymbol{B}^T\boldsymbol{\sigma}\, dx + \delta\boldsymbol{\xi}^T \left[\int_L \boldsymbol{G}\boldsymbol{\sigma}\, dx + \int_L \delta_{x_d}\boldsymbol{\sigma}\, dx\right]. \tag{7}$$

From the independence of the admissible variations $\delta\boldsymbol{d}$ and $\delta\boldsymbol{\xi}$, we obtain

$$\int_L \boldsymbol{G}\boldsymbol{\sigma}\, dx + \int_L \delta_{x_d}\boldsymbol{\sigma}\, dx = \boldsymbol{0}, \tag{8}$$

ensuring equilibrium between the traction $\boldsymbol{t} = \int_L \delta_{x_d}\boldsymbol{\sigma}\, dx$ acting on the discontinuity at $x = x_d$ and the stress resultant vector $\boldsymbol{\sigma} = \left[N_x\ N_y\ N_z\ M_x\ M_y\ M_z\right]^T$, N for force and M for moment w.r.t. x, y, z, in the bulk material at $x \neq x_d$, i.e., $\boldsymbol{t} = \boldsymbol{\sigma}$.

From the internal virtual work (7), we obtain the internal force

$$\boldsymbol{f}_{int} = \int_L \boldsymbol{B}^T\boldsymbol{\sigma}\, dx, \tag{9}$$

and a linearization with respect to the nodal displacement $\boldsymbol{d}$ yields the finite element stiffness matrix

$$\boldsymbol{K}_{uu} = \int_L \boldsymbol{B}^T\boldsymbol{C}\boldsymbol{B}\, dx \tag{10}$$

of the bulk material in (3). The constitutive model for the bulk material is

$$\boldsymbol{\sigma} = \boldsymbol{C}[\boldsymbol{B}\boldsymbol{d} + \boldsymbol{G}\boldsymbol{\xi}], \tag{11}$$

where $\boldsymbol{C} = \text{diag}\left[EA, kGA, kGA, EI_x, EI_y, EI_z\right]$ (see **Table 1**) is the structural elastic stiffness matrix of the bulk material. We use the simplest set of uncoupled linear elastic constitutive equations, which is based on the assumption that the beam cross-section possesses appropriate symmetries, e.g., see [14,15].

To evaluate the jump $\boldsymbol{\xi}$, we introduce the failure criteria

$$\Phi_i^F = |\sigma_i| - [\sigma_i^F + H_{ii}\beta_i] \quad ; \quad i = 1, \dots, 6 \text{ (no summation)} \tag{12}$$

for each degree of freedom, where $\sigma_i^F > 0$ is the failure limit (force or moment), $H_{ii} < 0$ is the structural softening modulus and $\beta_i > 0$ is an internal softening variable. The jump ξ_i is treated as the plastic strain in the standard implementation of elastoplasticity [16]. The structural softening modulus is then the structural tangent stiffness of the discontinuity, i.e.,

$$\dot{t}_i = H_{ii}\dot{\xi}_i = H_{ii}\dot{\xi}_i \quad ; \quad i = 1, \dots, 6 \text{ (no summation)}, \tag{13}$$

and the algorithm is summarized in **Table 1**.

The fracture energy required to break the beam is the area of the triangle below the softening part of the material response, starting at the peak value σ_i^F and ending at zero force/moment, i.e.,

$$G_f^i = \frac{1}{2}\frac{(\sigma_i^F)^2}{|H_{ii}|} \quad ; \quad i = 1, \dots, 6 \text{ (no summation)}. \tag{14}$$

Table 1: Return mapping algorithm for strain-softening. Quantities without indices are taken at the current time point $n+1$, $i = 1, \dots, 6$, and Einstein's summation convention does not apply. Here, γ_i is the consistency parameter.

1. **Load** $\xi_{i\,n}, \beta_{i\,n}$
2. **Compute trial force/moment and test for failure**

$$\boldsymbol{\varepsilon} = \boldsymbol{B}\boldsymbol{d}$$
$$\sigma_i^{trial} = C_{ii}[\varepsilon_i + G_{ii}\xi_{i\,n}]$$
$$\Phi_i^{F\,trial} = \left|\sigma_i^{trial}\right| - [\sigma_i^F + H_{ii}\beta_{i\,n}]$$

IF $\Phi_i^{F\,trial} \leq 0$ THEN
NO FAILURE $\sigma_i = \sigma_i^{trial}, \xi_i = \xi_{i\,n}, \beta_i = \beta_{i\,n}$
ELSE

3. **Return mapping**

WHILE $\Phi_i^{F\,trial} >$ THRESHOLD

$$\Delta\gamma_i = \frac{\Phi_i^{F\,trial}}{H_{ii} - C_{ii}G_{ii}} > 0 \text{ (denominator} > 0)$$
$$\sigma_i = \sigma_i^{trial} + C_{ii}G_{ii}\Delta\gamma_i \text{sign}(\sigma_i)$$
$$\xi_i = \xi_{i\,n} + \Delta\gamma_i \text{sign}\left(\sigma_i^{trial}\right)$$
$$\beta_i = \beta_{i\,n} + \Delta\gamma_i$$

END
ENDIF

For a more comprehensive description of the formulation and a coupling with plasticity, we refer to our recently accepted paper [1].

3 CASE STUDY

We consider a $18x18\ mm^2$ random fiber network with the fiber properties listed in **Table 2**. **Figure 1** shows the mechanical response of a random fiber network with the sheet density $\rho_s = 1450\ kg/m^3$ and $\rho_s = 450\ kg/m^3$, $\rho_f = 1500\ kg/m^3$ is the fiber density. **Figures 2-3** show the evolution of the norm of the jump, $|\boldsymbol{\xi}|$, at the points A-D and E-F in **Fig. 1**. In the selected tensile load case, only mode I fiber fractures appear, i.e., $\xi_i = 0$ for $\xi_{i\neq 1}$. We use one element between two fiber-to-fiber intersections.

Table 2: Fiber properties.

Young's modulus, $E\ [MPa]$	6500
Shear modulus, $G\ [MPa]$	$E/2$
Shear correction factor, k	0.84
Tensile strength, $\sigma_F\ [MPa]$	840
Fracture energy, $G_f\ [Nmm]$	0.4
Cross-section area, $A\ [mm^2]$	$3.63\text{e}-04$
Shear correction factor, k	0.84
Polar moment of inertia, $I_x\ [mm^4]$	$3.66\text{e}-08$
Area moment of inertia, $I_y\ [mm^4]$	$3.29\text{e}-08$
Area moment of inertia, $I_z\ [mm^4]$	$3.66\text{e}-09$
Failure limit, $\sigma_i^F; i = 1, \ldots, 6$	$A\sigma_F$
Fiber length, $L^f\ [mm]$	2.5

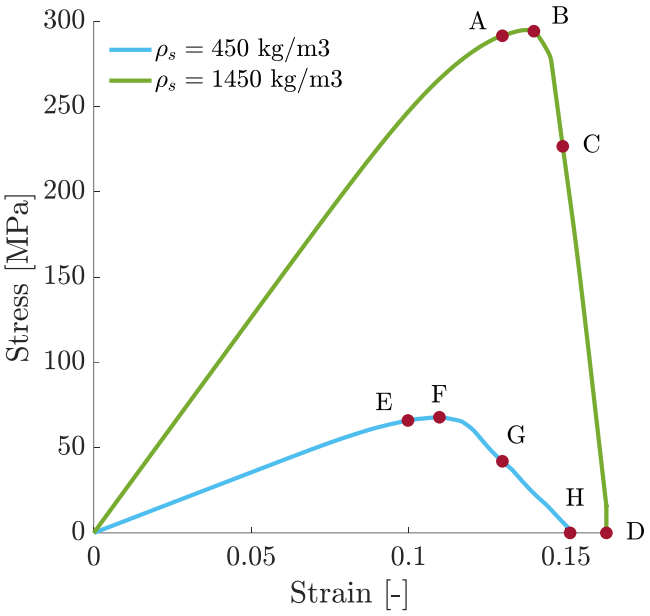

Fig. 1: Mechanical response of a random fiber network loaded in tension. The sheet density is $\rho_s = 1450\ kg/m^3$ (green) and $\rho_s = 450\ kg/m^3$ (blue), respectively, $\rho_f = 1500\ kg/m^3$ is the fiber density.

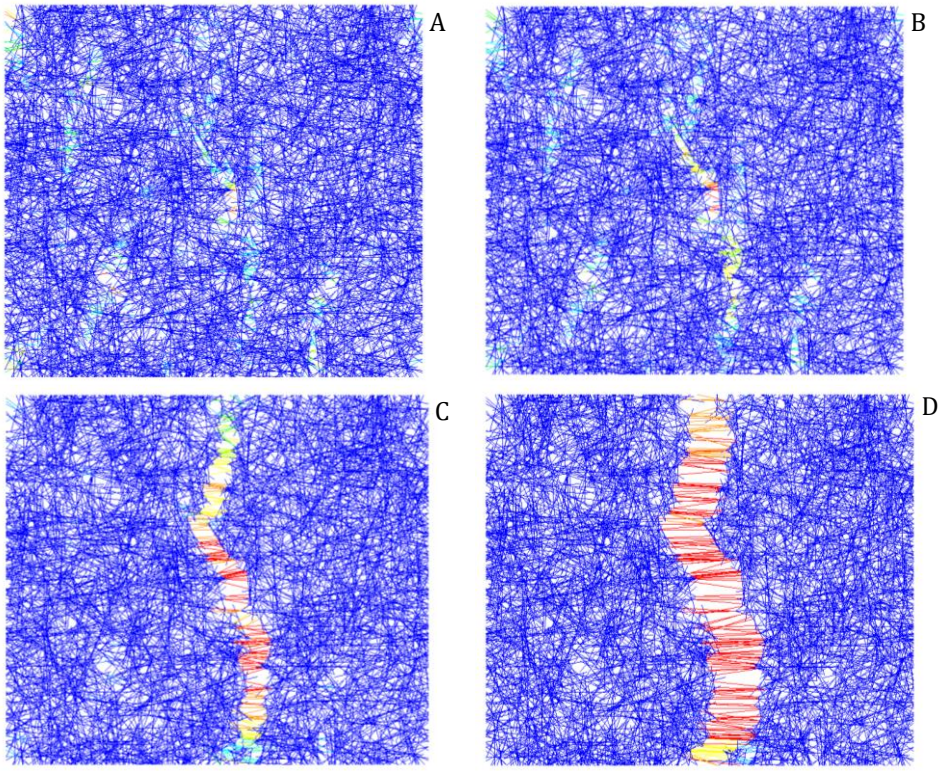

Fig. 2: Norm of crack opening displacement $|\boldsymbol{\xi}|$ at points A-D in **Fig. 1**, showing multi-fracturing fibers in a random fiber network loaded in tension. The minimum value is zero and colored blue, while the maximum value is colored red and evolves from A to D as 0.18; 0.31; 0.98; 2.15 $[mm]$, respectively.

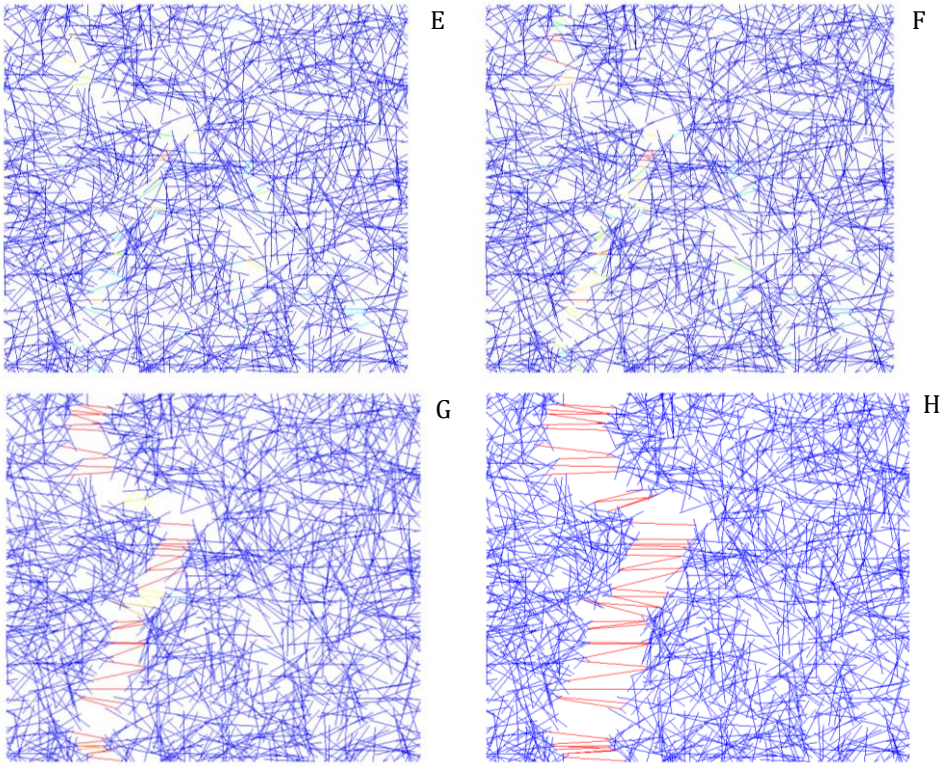

Fig. 3: Norm of crack opening displacement $|\boldsymbol{\xi}|$ at points E-H in **Fig. 1**, showing multi-fracturing fibers in a random fiber network loaded in tension. The minimum value is zero and colored blue, while the maximum value is colored red and evolves from E to H as $0.14; 0.26; 1.27; 2.62$ $[mm]$, respectively.

4 CONCLUSIONS

- We propose a staggered solution scheme for the embedded strong discontinuity finite element method applied to fracture of beam structures, e.g., see our recently accepted paper [1].
- We demonstrate the robustness of our implementation for modeling multi-fracturing fibers in random fiber networks loaded in tension.
- Our implementation enables a user-friendly integration into commercial finite element software (in the present study ANSYS).
- The FORTRAN source code is freely available to benchmark our implementation.

REFERENCES

[1] V. Tojaga, A. Kulachenko, S. Östlund, T.C. Gasser, Modeling multi-fracturing fibers in fiber networks using elastoplastic Timoshenko beam finite elements with embedded strong discontinuities - Formulation and staggered algorithm, Comput. Methods Appl. Mech. Eng. (2021).

[2] J.C. Simo, J. Oliver, F. Armero, An analysis of strong discontinuities induced by strain-softening in rate-independent inelastic solids, Comput. Mech. (1993). https://doi.org/10.1007/BF00372173.

[3] M. Nikolic, A. Ibrahimbegovic, Rock mechanics model capable of representing initial heterogeneities and full set of 3D failure mechanisms, Comput. Methods Appl. Mech.

Eng. (2015). https://doi.org/10.1016/j.cma.2015.02.024.
[4] D. Ehrlich, F. Armero, Finite element methods for the analysis of softening plastic hinges in beams and frames, Comput. Mech. (2005). https://doi.org/10.1007/s00466-004-0575-z.
[5] M. Nikolić, E. Karavelić, A. Ibrahimbegovic, P. Miščević, Lattice Element Models and Their Peculiarities, Arch. Comput. Methods Eng. (2018). https://doi.org/10.1007/s11831-017-9210-y.
[6] J. Čarija, M. Nikolić, A. Ibrahimbegovic, Ž. Nikolić, Discrete softening-damage model for fracture process representation with embedded strong discontinuities, Eng. Fract. Mech. (2020). https://doi.org/10.1016/j.engfracmech.2020.107211.
[7] M. Nikolic, A. Ibrahimbegovic, P. Miscevic, Brittle and ductile failure of rocks: Embedded discontinuity approach for representing mode I and mode II failure mechanisms, Int. J. Numer. Methods Eng. (2015). https://doi.org/10.1002/nme.4866.
[8] E. Karavelić, M. Nikolić, A. Ibrahimbegovic, A. Kurtović, Concrete meso-scale model with full set of 3D failure modes with random distribution of aggregate and cement phase. Part I: Formulation and numerical implementation, Comput. Methods Appl. Mech. Eng. (2019). https://doi.org/10.1016/j.cma.2017.09.013.
[9] F. Armero, D. Ehrlich, Numerical modeling of softening hinges in thin Euler-Bernoulli beams, Comput. Struct. (2006). https://doi.org/10.1016/j.compstruc.2005.11.010.
[10] A. Ibrahimbegovic, Nonlinear solid mechanics, Solid Mech. Its Appl. (2009). https://doi.org/10.1007/978-90-481-2331-5_1.
[11] I. Bitar, P. Kotronis, N. Benkemoun, S. Grange, A generalized Timoshenko beam with embedded rotation discontinuity, Finite Elem. Anal. Des. (2018). https://doi.org/10.1016/j.finel.2018.07.002.
[12] A. Ibrahimbegovic, S. Melnyk, Embedded discontinuity finite element method for modeling of localized failure in heterogeneous materials with structured mesh: An alternative to extended finite element method, Comput. Mech. (2007). https://doi.org/10.1007/s00466-006-0091-4.
[13] A. Kulachenko, T. Uesaka, Direct simulations of fiber network deformation and failure, Mech. Mater. (2012). https://doi.org/10.1016/j.mechmat.2012.03.010.
[14] A. Ibrahimbegović, On finite element implementation of geometrically nonlinear Reissner's beam theory: three-dimensional curved beam elements, Comput. Methods Appl. Mech. Eng. (1995). https://doi.org/10.1016/0045-7825(95)00724-F.
[15] Y. Luo, An Efficient 3D Timoshenko Beam Element with Consistent Shape Functions, Adv. Theor. Appl. Mech. (2008).
[16] J.C. Simo, T.J.R. Hughes, Computational Inelasticity, 1st ed., Springer-Verlag New York, 1998. https://doi.org/10.1007/b98904.